Supporting Information for:

Crucial Role of Nuclear Dynamics for Electron Injection in a Dye-Semiconductor Complex

Adriano Monti[‡], Christian F.A. Negre[††], Victor S. Batista[†], Luis G. C. Rego[§], Huub J.M. de Groot[‡], Francesco Buda[‡]

[‡]_Leiden University, Leiden Institute of Chemistry, Einsteinweg 55, 2300 RA, Leiden, The Netherlands_

[†]_Department of Chemistry, Yale University, P.O. Box 208107, New Haven, Connecticut, United States_

[††]_Theoretical Division, Los Alamos National Laboratory, Los Alamos, New Mexico 87545, United States_

[§]_Department of Physics, Universidade Federal de Santa Catarina, Florianópolis, SC 88040-900, Brazil_

**E-mail corresponding author:** f.buda@chem.leidenuniv.nl

TABLE OF CONTENTS

SI-1. Optimization of the Extended Hückel parameters

In the quantum dynamics calculations, the electronic properties of the system are described by means of a tight-binding Hamiltonian based on the extended Hückel (EH) theory[1,2]. This method employs as basis set nonorthogonal Slater-type orbitals (STO) centered at different atoms. The molecular orbitals (MO) are constructed as linear combinations of the STO atomic orbitals (AO) as $\psi_j = \sum_{v=1}^{N} c_{vj} \varphi_v$. It follows that the coefficients c_{vj} are obtained by solving the generalized eigenvalues equation $HC_j = \varepsilon_j S C_j$. The diagonal elements H_{ii}^0 of the **H** matrix, also called Coulomb integrals, represent approximately the valence state oxidation potentials of the atomic species i, and their value is assigned through parameterization. The off-diagonal elements $H_{im}^0 = \frac{1}{2} k_{im}(H_{ii} + H_{mm}) S_{im}$ (or resonance integrals) represent the energy of the electron in the region where the two atomic orbitals i and m overlap (S_{im}). k_{im} are the modified empirical Wolfsberg-Helmholz parameters[2,3]. The matrix elements of the tight-binding EH Hamiltonian are therefore dependent on three semiempirical parameters: H_{ii}^0, k_{im} and the effective charge of the nucleus (ζ) embedded in the definition of the STOs. In this work, the optimization of the standard EHT parameters is performed only for the chemical species belonging to the organic chromophores; details of the method are provided ahead. Initially, the density of states (DOS) for the (110) surface of anatase is obtained with the standard EH parameters[4] imposing periodic boundary conditions along the [101] and the [010] directions. For the calculation of the isolated TiO$_2$ surface, as well as for the functionalized one, an orthorhombic supercell with lattice parameters a=10.239 Å, b=15.137 Å and c=40 Å is used. As can be seen in Figure S1 below, the standard EH calculation estimates the lower edge of the TiO$_2$ conduction band (CB) to begin at -10 eV. Although it is experimentally difficult to assign an exact estimate to this parameter, -4.0 eV (vs. vacuum) is commonly found as approximated value for the onset of the TiO$_2$ CB[5,6].

Figure S1. Density of states of a two layers (101) anatase slab obtained through electronic structure calculations with standard EH parameters.
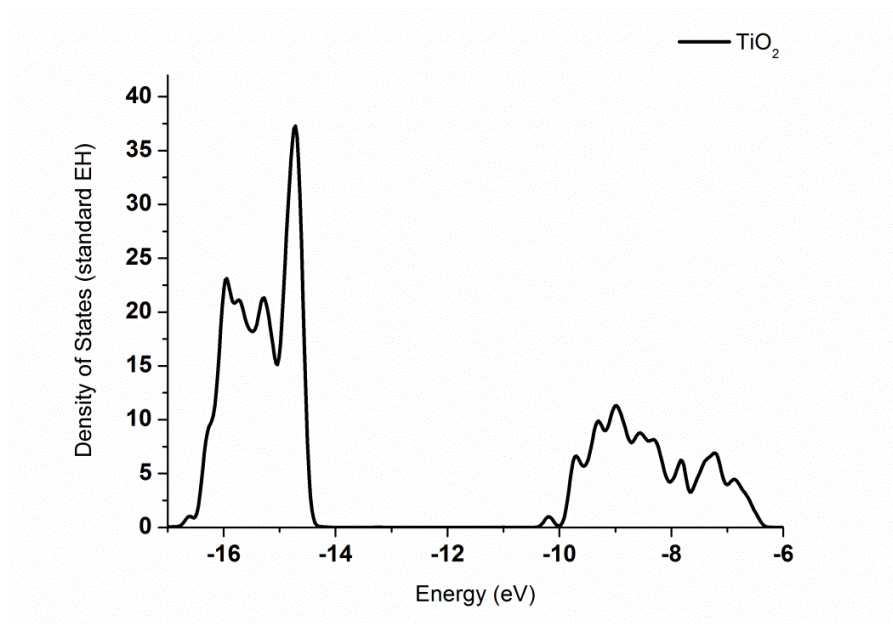
At the same time, the chromophore geometries are optimized in their ground state within the DFT level of theory, using the exchange correlation functional B3LYP[7] coupled with the cc-pVDZ basis set. These calculations are performed with the Gaussian09 software package[8]. In order to obtain the correct energy gradient with respect to the semiconductor CB edge, the DFT frontier molecular orbital (FMO) energy values are down shifted of 6 eV. These corrected energies are used as target values for the optimization of the EH parameters.

The optimization is performed using a cost function of the form $f(\{\zeta\},\{H_{ii}^0\},\{k\}) = \sum_{j=1}^{M} \omega_j \left[P_j(\{\zeta\},\{H_{ii}^0\},\{k\}) - P_j^{ref}\right]^2$, where $P_j(\{x\})$ is the system's property of interest, P_j^{ref} the target value for that property and ω_j the relative weight of the constraint. For the present work we constrain only the energy values for the highest occupied molecular orbital (HOMO), the lowest and the second lowest unoccupied molecular orbital (LUMO and LUMO+1) of the dye molecules. The shifted DFT energies are used as target values. The comparison between the
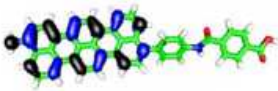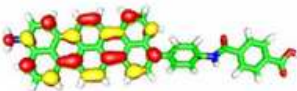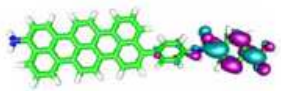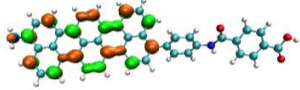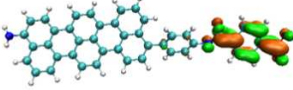
symmetry of the orbitals obtained with DFT/B3LYP and Extended Hückel is also used to evaluate the quality of the optimized parameters.

The results of the calculations performed with the semi empirical and the *ab* initio methods are compared in Table S1 and Table S2 below. These results validate the use of the optimized set of EH parameters for the electronic description of the investigated complexes.

Table S1. Comparison between the frontier molecular orbital (FMO) energies obtained with the DFT/B3LYP method, the target values for the EH parameters optimizations, and the FMO energies calculated with the optimized EH parameters. The target values are estimated by applying a rigid 6 eV down shift to the DFT/B3LYP energy values.

		DFT/B3LYP (eV)	Target values (eV)	Optimized EH (eV)
	HOMO	-4. 7	-10.7	-10.7
T-AM	LUMO	-2.6	-8.6	-8.6
	LUMO+1	-2.4	-8.4	-8.3

Table S2. Comparison between the FMO of the T-AM molecule calculated in vacuum at the DFT/B3LYP and at the Extended Hückel level of theory.

	HOMO	**LUMO**	**LUMO+1**
DFT/B3LYP			
Optimized EH parameters			

SI-2. <u>Quantum dynamics propagation of the hole and electron wave packets</u>

In this study, the processes of charge transfer are studied by combining quantum electronic and classical molecular dynamics methods. This technique has already been applied for the description of charge transfer processes in previous works, where more theoretical details can also be found[9–11]. Here we present only the basics of the theoretical approach.

The quantum propagation of the hole/electron wave packet is performed either on a static nuclear geometry or along a classical nuclear dynamics trajectory obtained a priori.

The initial wave packet for the hole and the electron are set as the HOMO and the LUMO of the adsorbate molecule and can be written as a linear combination of position dependent localized atomic orbitals (AO) $|\Psi(0)\rangle = \sum_\varphi^{ABS} C_\varphi(0) |\varphi(0)\rangle$. These AO are used to build up the tight-binding Hückel Hamiltonian matrix elements H_{ij}. Diagonalization of this Hamiltonian produces the adiabatic basis of delocalized molecular orbitals (MO). The transformation of the wavepacket from AO to MO basis set can be achieved using the transformation operator $\hat{P} = \sum_\psi \sum_{\varphi,\chi} |\varphi\rangle (S^{-1}) \langle\chi|\psi\rangle\langle\psi| = \sum_{\varphi,\psi} C_{\varphi,\psi} |\varphi\rangle\langle\psi|$.

If it is assumed that the nuclei do not change their positions, the Hamiltonian H_{ij} matrix elements do not evolve in time. Therefore, solving the time-dependent Schrödinger equation for the wave packet $|\Psi(t)\rangle = \sum_\psi C_\psi(t) |\psi(t)\rangle$ in the MO basis leads to the solution $C_\psi(t) = C_\psi(0) \exp(-iE_\psi t/\hbar)$, where the phase of the wave packet coefficients $C_\psi(t)$ are the only quantities evolving in time.

However, this static approximation is valid only within a timeframe where nuclear vibrations can be disregarded (< 30 fs). For longer simulations, nuclear dynamics ought to be taken into account.

In this work, the nuclear trajectory for the isolated molecule is calculated beforehand through *ab initio* Molecular Dynamics using the Car-Parrinello MD (CPMD) code[12]. The DFT/B3LYP optimized geometry is used as starting point for the MD simulation, which is carried out in vacuum using the pseudopotential of reference[13] with a plane wave cut-off of 70 Rydberg and the BLYP[14] exchange correlation functional. Applying the Nosé-Hoover thermostat the molecules are brought at a temperature of 300 K and allowed to equilibrate for 2 ps using a time step of 0.1 fs. During the whole simulation, the atoms of the carboxylic acid anchoring group are constrained in their initial positions. At the end of the simulation the carboxylic acid is replaced with the previously optimized TiO_2 slab already functionalized with the anchoring unit.

Once the nuclear trajectory is obtained for the chromophore, the hole and the electron wave packets are propagated along this trajectory following the combined AO/MO time-propagation method[11,16]. When the nuclear coordinates change, the position dependent atomic orbitals become time dependent, inducing a time dependence also in the Hamiltonian $H_{ij}(t)$. The solution of the time dependent generalized eigenvalue equation $H\psi = ES\psi$ at each time step produces the adiabatic molecular orbitals $|\psi(t)\rangle$ of the entire system. In this work, the time step used for the quantum dynamics is the same used for the MD trajectory, $\delta\tau = 0.1$ fs. Within the time slice $\delta\tau$ the MO basis functions and the EH Hamiltonian are treated as time independent. Thus the wavepacket is time evolved in the MO basis representation. At the end of the time slice the evolved wavepacket undergoes a unitary transformation back to the AO basis: $|\Psi(\delta\tau)\rangle = \sum_{\varphi} C_{\varphi}(\delta\tau) |\varphi(0)\rangle$. The new coefficients of the wavepacket $C_{\varphi}(\delta\tau)$ are passed to the next MD nuclear configuration.

This methodology has been already applied for the description of heterogeneous electron transfer processes[9,15]. A detailed description of the methodology with explanation of the electron-nuclear coupling dynamics can be found in Ref.[16].

SI-3. Test on geometrical relaxation in the excited state

An additional test has been performed to check the effects of the photo-excitation on the T-AM chromophore. Using the CAM-B3LYP exchange-correlation functional with a cc-pVDZ basis set, we have optimized the geometry of the T-AM dye in the first excited state, which has a dominant HOMO-LUMO character. The optimized geometry in the excited state shows only small changes in the C-C bond lengths of the terrylene antenna with maximum displacements of ~0.03 Å. Given that the LUMO is highly localized on the terrylene, not surprisingly these geometrical changes are only observed in the terrylene molecule and do not propagate on the AM bridge whose geometry is essentially not modified by the excitation. These results strongly suggest that the dynamics of the AM bridge will be hardly affected by the excitation localized on the terrylene antenna, giving further justification to the use of a ground state dynamics for the study of the electron injection.

Figure S2. Electron and hole time-dependent survival probability profiles of system T-AM-TiO₂ (blue and green line, respectively). The quantum dynamic evolution of the wavepackets is performed on a fixed set of molecular coordinates (ground-state optimized geometry) using EH parameters optimized against DFT/B3LYP results. The time step of the simulation is δτ=0.1fs.
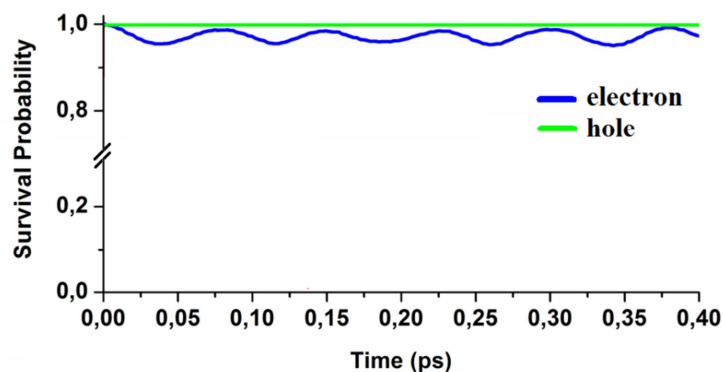

Figure S3. Localization of the Electron Donor and Electron Acceptor states along the T-AM-TiO₂ MD trajectory. On the right hand side are reported the MD time frames and the value of the dihedral angle α corresponding to the two electronic states shown.
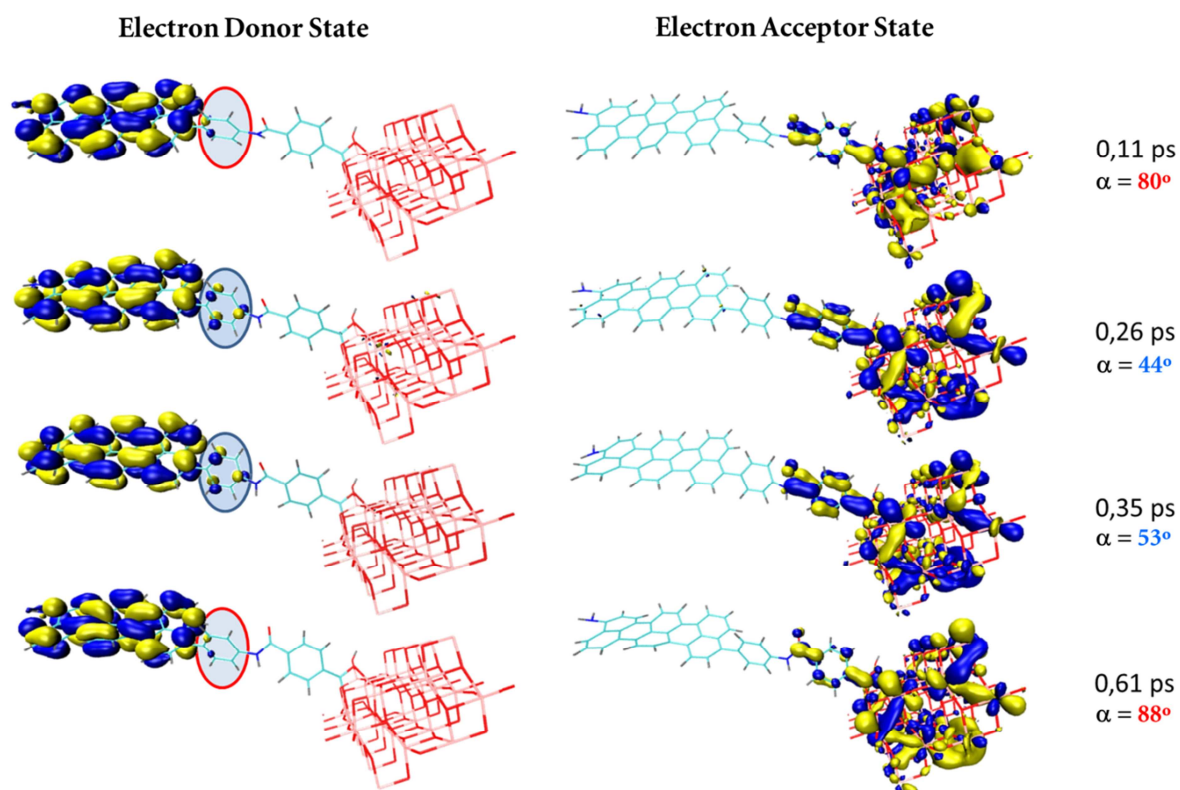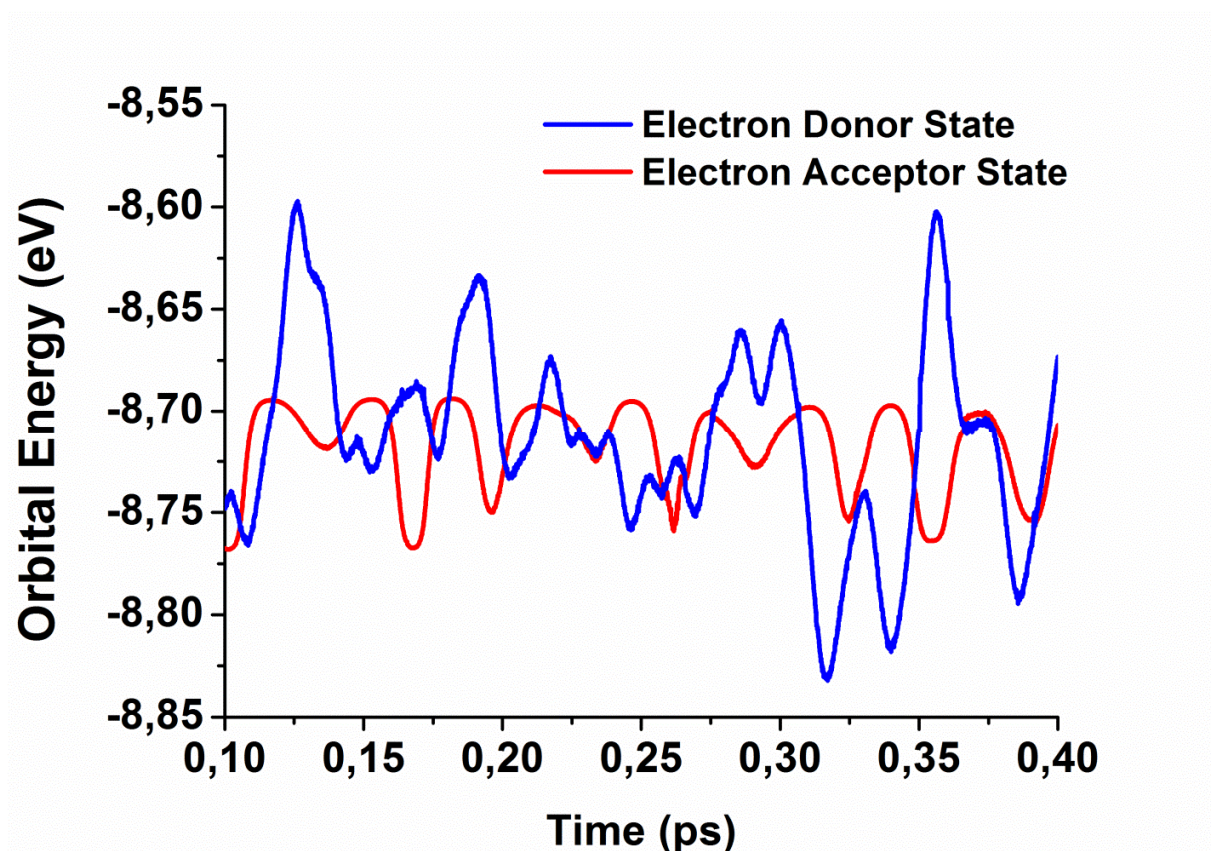
Figure S4. Energy values of the Electron Donor and the Electron Acceptor orbitals along a portion of the EQD simulation.


SI-4. Test on T-Stilbene-TiO$_2$

The survival probability reported in Figure 2 and Figure 3 shows a constant decrease of the electron wavepacket localized on T-AM. This indicates the absence of large charge fluctuations from the semiconductor back onto the donor state of the dye. To verify that this is due to the AM bridge rectification properties, following the same computational procedure used for T-AM – TiO$_2$, we perform an EQD simulation for a system in which we substitute the AM bridge with the fully conjugated (E)-stilbene molecule (Figure S5 a). Due to its conjugation this system is not expected to show rectification[17].

The results for T-Stilbene-TiO$_2$ are reported in Figure S5 b. Due to the fully conjugated nature of (E)-stilbene, the initial wavepacket is localized not only on the terrylene but on the entire dye. In this case the electron injection is extremely fast, due to the strong coupling with the semiconductor conduction band states (see Figure S5 b, first 20 fs). However, along the dynamics the survival probability for T-Stilbene-TiO$_2$ shows strong fluctuations associated with electron density fluctuation between the antenna and the semiconductor (see insets in Figure S5 b). This is a strong indication that the T-Stilbene-TiO$_2$ system does not show rectification capability in contrast to the results shown for T-AM-TiO$_2$.

Figure S5. (a) Schematic representation of the T-Stilbene dye. (b) SP profile of the EQD simulation of T-Stilbene-TiO2 along an MD trajectory. The insets show the wavepacket localization at different snapshots along the EQD.
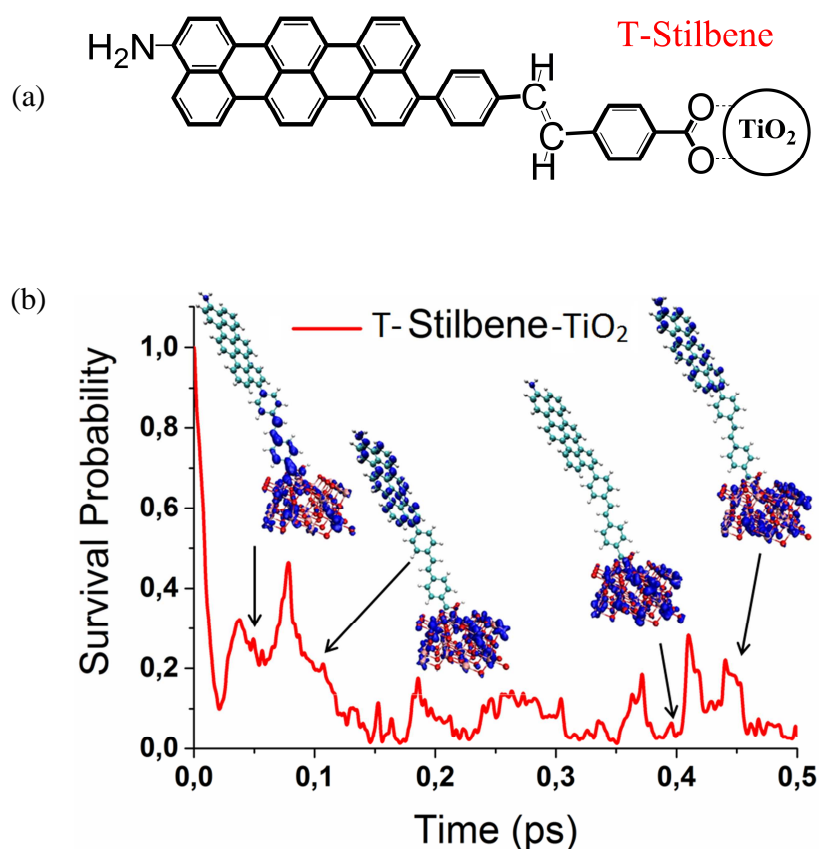
REFERENCES

(1)   Hoffmann, R. An Extended Hückel Theory. I. Hydrocarbons. *J. Chem. Phys.* **1963**, *39*, 1397–1412.

(2)   Ammeter, J. H.; Buergi, H. B.; Thibeault, J. C.; Hoffmann, R. Counterintuitive Orbital Mixing in Semiempirical and Ab Initio Molecular Orbital Calculations. *J. Am. Chem. Soc.* **1978**, *100*, 3686–3692.

(3)   Wolfsberg, M.; Helmholz, L. The Spectra and Electronic Structure of the Tetrahedral Ions MnO4–, CrO4––, and ClO4–. *J. Chem. Phys.* **1952**, *20*, 837–843.

(4)   Santiago Alvarez. Table of Parameters for Extended Huckel Calculations, Collected by Santiago Alvarez, Universitat de Barcelona (1995). **1995**.

(5)   Ding, W.-L.; Wang, D.-M.; Geng, Z.-Y.; Zhao, X.-L.; Yan, Y.-F. Molecular Engineering of Indoline-Based D–A−π–A Organic Sensitizers toward High Efficiency Performance from First-Principles Calculations. *J. Phys. Chem. C* **2013**, *117*, 17382–17398.

(6)   Edvinsson, T.; Pschirer, N.; Schöneboom, J.; Eickemeyer, F.; Boschloo, G.; Hagfeldt, A. Photoinduced Electron Transfer from a Terrylene Dye to TiO2: Quantification of Band Edge Shift Effects. *Chem. Phys.* **2009**, *357*, 124–131.

(7)   Becke, A. D. Density-functional Thermochemistry. III. The Role of Exact Exchange. *J. Chem. Phys.* **1993**, *98*, 5648–5652.

(8)   M. J. Frisch, G. W. Trucks, H. B. Schlegel, G. E. Scuseria, M. A. Robb, J. R. Cheeseman, G. Scalmani, V. Barone, B. Mennucci, G. A. Petersson, et al. *Gaussian 09, Revision D.01*; Gaussian, Inc.: Wallingford CT, 2009.

(9)   Hoff, D. A.; da Silva, R.; Rego, L. G. C. Coupled Electron–Hole Quantum Dynamics on D−π–A Dye-Sensitized TiO2 Semiconductors. *J. Phys. Chem. C* **2012**, *116*, 21169–21178.

(10)   Rego, L. G. C.; Hames, B. C.; Mazon, K. T.; Joswig, J.-O. Intramolecular Polarization Induces Electron–Hole Charge Separation in Light-Harvesting Molecular Triads. *J. Phys. Chem. C* **2014**, *118*, 126–134.

(11)   Hoff, D. A.; Silva, R.; Rego, L. G. C. Subpicosecond Dynamics of Metal-to-Ligand Charge-Transfer Excited States in Solvated [Ru(bpy)3]2+ Complexes. *J. Phys. Chem. C* **2011**, *115*, 15617–15626.

(12)   *CPMD, Http://www.cpmd.org/, Copyright IBM Corp 1990-2008, Copyright MPI fürFestkörperforschung Stuttgart 1997-2001*.

(13)   Lin, I.-C.; Coutinho-Neto, M. D.; Felsenheimer, C.; von Lilienfeld, O. A.; Tavernelli, I.; Rothlisberger, U. Library of Dispersion-Corrected Atom-Centered Potentials for Generalized Gradient Approximation Functionals: Elements H, C, N, O, He, Ne, Ar, and Kr. *Phys. Rev. B* **2007**, *75*, 205131.

(14)   Becke, A. D. Density-Functional Exchange-Energy Approximation with Correct Asymptotic Behavior. *Phys. Rev. A* **1988**, *38*, 3098–3100.

(15)   Abuabara, S. G.; Rego, L. G. C.; Batista, V. S. Influence of Thermal Fluctuations on Interfacial Electron Transfer in Functionalized TiO2 Semiconductors. *J. Am. Chem. Soc.* **2005**, *127*, 18234–18242.

(16)   Da Silva, R.; Hoff, D. A.; Rego, L. G. C. Coupled Quantum-Classical Method for Long Range Charge Transfer: Relevance of the Nuclear Motion to the Quantum Electron Dynamics. *J. Phys. Condens. Matter* **2015**, *27*, 134206.

(17)   Ding, W.; Negre, C. F. A.; Vogt, L.; Batista, V. S. Single Molecule Rectification Induced by the Asymmetry of a Single Frontier Orbital. *J. Chem. Theory Comput.* **2014**, *10*, 3393–3400.